Indonesian Journal of Biotechnology

VOLUME 28(2), 2023, 94-101 | RESEARCH ARTICLE

Electrochemical performance of plant trace element incorporated silver nanoparticles synthesis from *Datura metel* L.

Karuppiah Chinniah[1], Karthik Kannan[2], Vivek Maik[3], Vladmir Potemkin[4], Maria Grishina[4], Samuel Johnson Christopher Jeyaseelan[5], Arumugam Muthuvel[6], David Gnanasangeetha[7], Krishnamoorthy Gurushankar[1,4,*]

[1]International Research Centre, Kalasalingam Academy of Research and Education, Krishnankoil, Virudhunagar, Tamilnadu, India - 626 126
[2]Chemical Sciences Department and the Radical Research Center, Ariel University, Ariel 40700, Israel
[3]Department of Electronics and Communication Engineering, Kattankulathur Campus, SRM Institute of Science and Technology, Chennai
[4]Laboratory of Computational Modelling of Drugs, Higher Medical and Biological school, South Ural State University, Chelyabinsk-454080, Russia
[5]PG Department of Physics, Mannar Thirumalai Naicker College, Madurai, 625004, Tamilnadu, India
[6]Department of Physics, Theivanai Ammal College for Women (Autonomous), Villupuram, Tamil Nadu-605602, India
[7]Department of Chemistry, PSNA College of Engineering and Technology, Dindigul, 624622, Tamil Nadu, India
*Corresponding author: gurushankar01051987@gmail.com

SUBMITTED 14 July 2022 **REVISED** 23 January 2023 **ACCEPTED** 8 March 2023

ABSTRACT In our report, silver nanoparticles (AgNPs) were prepared from the leaf extract of *Datura metel* L. via the green synthesis method. *Datura metel* L. is a herbal medicinal plant from the Solanaceae family. The as-prepared AgNPs were characterized using UV-Vis spectrometer, X-ray Diffraction (XRD), Fourier Transform Infrared (FTIR) spectroscopy and Scanning Electron Microscopy (SEM) with Energy Dispersive X-ray (EDAX) analysis. The peak appearance of a Surface Plasmon Resonance (SPR) at 415 nm suggested the creation of AgNPs in the UV-Vis spectrum. The XRD pattern showed the face-centered cubic crystal structure of AgNPs with organometallic complex phase. Based on the FTIR spectrum, the peaks revealed the existence of biomolecules. SEM images showed the shape of the clastic rocks and the EDAX profile authenticated the presence of Ag and plant trace element. The cyclic voltammetry, Chronopotentiometry, and electrochemical impedance spectroscopy analysis were performed on an as-prepared Ag electrode. A specific capacitance of 267.59 F/g at 0.5 A/g and a cyclic retention of 83.7% after 5000 charge-discharge cycles were obtained. Hence, this material could be utilized in supercapacitor energy storage devices.

KEYWORDS *Datura metel* L.; Green synthesis; Organometallic complex phase; Plant trace element; Silver nanoparticles (AgNPs); Supercapacitor

1. Introduction

Medicinal plants are most useful for discovering drugs for every disease from their traditional period to COVID-19 (Gurushankar et al. 2020; Muthuvel et al. 2021). The scientific standard limitations of bioactive compounds and trace element intake are still unclear. However, low levels of trace elements, such as Mg, Na, S, Zn, Ni, Fe, Cu, and Cl are causing severe deficiency in the human physiological system (Khan et al. 2007). Nanoscale silver is considered a remarkable bioactive material for biological applications due to its high light absorption and size depending on its interacting ability (Adavallan et al. 2017; Chinnaiah et al. 2021).

Datura metel L. is an herbal medicinal plant of the Solanaceae family that has been employed for asthma, anesthetic and tumor convulsions in traditional periods of India. Our previous research group tested the CDK4 inhibitory potential of the newly found baimantuoluoamide A and baimantuoluoamide B isolated from *D. metel*. Baimantuoluoamide B was discovered to be a very potent CDK4 inhibitor with unique structural properties based on the molecular dynamics data. The MM/GBSA method was used to examine the baimantuoluoamide B binding on a per-residue basis and the top donating amino acid residues was found. The findings showed that baimantuoluoamide B is a promising hit molecule that can be used to grow selective CDK4 inhibitors in the future (Gurushankar et al. 2021). Based on the theoretical efficacy, analyze their experimental capability for nanoparticle synthesis using *D. metel*. Hence, utilization of *Datura* species increased for several research applications (Stephane et al. 2020; Tan et al. 2020) since the natural withanolides are present as a major chemical constitution in their secondary

metabolism. The α, β-unsaturated del lactones ring in their side chain facilitates an easy chemical defense mechanism with oxygen, which can prepare non-toxic nanoparticles without additional reducing agents with hazardous chemical compounds. Recently, Cu_2O nanoparticles using *D. metel* prepared via the green synthesis method and its various characterization along with alkaloids compounds, such as hyoscyamine and atropine, stabilization studied by the DFT method (Chinnaiah et al. 2022). Among the metal nanoparticles, Ag is a primary conductive material with low cost, compared to Au, for many applications and is foremost adopted for green synthesis. It has several advantages compared to the existing nanoparticle synthesis, including being eco-friendly, easy to manage, and less energy required. Hence, energy storage nanomaterials synthesis green technologies are increasing day by day. Due to the motivation of the present study, AgNPs have been synthesized by leaf extract of *D. metel* through the green synthesis method. The prepared AgNPs characterized by various analytical techniques and evaluated their electrochemical performance.

2. Materials and Methods

Datura metel L. was collected from the agricultural land of Krishnankoil, Tamil Nadu, India, and silver nitrate (99.5% purity) was purchased from SRL Chemicals Mumbai, India.

In this process, 10 mg of homogeneous *D. metel* was washed with tap water to avoid dust particles and cut into small pieces. The leaves were poured into 100 mL of distilled water and a stirrer for 50 min at 70 °C. After cooling, the extract was filtered using Whatman No.1 filter paper with a pore size of 25 nm then the filtered extract was used to synthesize the AgNPs. 10 mL of leaf extract was added drop by drop with 0.2 M of silver nitrate solution. The reaction mixture was allowed for 5 min stirring, getting the colloidal yellow color solution, which indicates a reduction of Ag^+ ions into Ag^0 ions. The binary mixture of the solution was continuously stirred for 90 min at 40 °C. Subsequently, the reaction showed the color difference from light yellow to dark brown when kept at room temperature. The obtained precipitate was centrifuged at 2,000 rpm for 1 h and then washed with doubled deionized water and ethanol. The prepared sample was dehydrated at 100 °C and employed for further characterization. The following Tauc's plot equation is used to calculate the band gap of the Ag nanoparticles.

$$\mathrm{h}\nu\alpha = A(h\nu - E_g)^{1/2} \quad (1)$$

Where Eg is band gap energy, ν is frequency, α-absorption co-efficient, and h is plank constant. The Scherer formula is used to calculate the crystallite size of the obtained AgNPs.

$$\mathrm{D} = k\lambda/\beta cos\theta \quad (2)$$

Where, D indicates crystallite size, k is Scherer's constant (k=0.94), λ denotes the wavelength of the X-ray used (1.5406 Å), β is known as full-width half-maximum (FWHM), and θ is Bragg's angle. The specific capacitance of the Ag electrode is worked out from the CV curves according to the below equation (33).

$$\mathrm{C_{sp}(CV)} = \frac{\int ldv}{sm\Delta V}F \quad (3)$$

Where C_{sp} represents the specific capacitance of the fabricated electrode, I represents the current, s describes the voltage, m represents the mass of the working electrode and ΔV describes the scan rates. The specific capacitance of the prepared electrode was calculated from the GCD curves employed by the below mathematical expression.

2.1. Electrochemical analysis

The supercapacitor performance of synthesized AgNPs created an electrode material. It has been analyzed on an electrochemical workstation [model-CH 60008E, CH instrument, USA] with a conventional three-electrode system. In this system, (Ag/AgCl) is the reference electrode, platinum wire is the counter electrode and AgNPs overlay on Ni foil as the working electrode. The reference electrode, counter electrodes, and prepared working electrodes are submerged in 30 mL of aqueous electrolyte solution, accounting for 1 M KOH and their measured pH value is 13. The analytical balance used to measure the loading mass of the Ag NPs on Ni foil and the prepared electrochemical system (Ag electrode + 1 M KOH) was used for electrochemical analysis. Then a performance of CV, Choronopotentiometry and EIS of Ag electrode was analyzed in a three-electrode system.

2.2. Electrode preparation

According to the Dr. blade technique (Karuppiah et al. 2021) Ag electrode was developed by mixing synthesized Ag nanopowder, activated carbon, polyvinylidene difluoride (PVDF) as a binder in the 80:10:10 mass ratio and sludge using NMP (N - methyl pyrrolidinone) as a solvent was generated, then coated on 1 cm^2 square Ni foil and dried at 70 °C for 12 h. Well-coated Ag NPs on Ni foil are now used as a working electrode for electrochemical analysis.

3. Results and Discussion

3.1. UV-Vis spectroscopy analysis

Perkin Elmer spectrometer was used to analyze the optical properties of AgNPs, and the sample was examined at the spectrum of 200-900 nm. The synthesised AgNPs, with a characteristic peak at 410 nm (Figure 1a) was caused by the Surface Plasmon Resonance (SPR) absorption band. It can be observed by intensity changes from light yellow colour to dark brown colour during the synthesis as illustrated in Figure 1(a,c) because of the vibration of d electrons of metal nanoparticles in resonance with a light

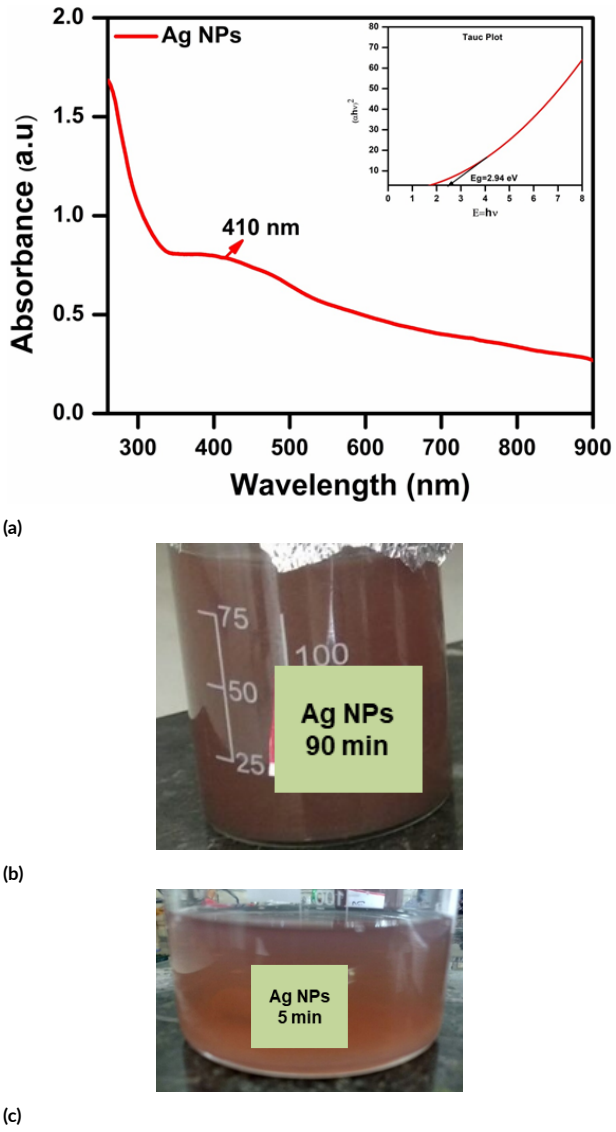

FIGURE 1 UV-Vis spectroscopy analysis of AgNPs.

wave. According to the Tauc plot study, the band gap of AgNPs is 2.94 eV (Figure 1). This band gap reveals the quantum confinement effect of AgNPs (Mistry et al. 2021). The synthesized AgNPs with this large band gap further can be used in optoelectronic devices such as batteries and sensors.

3.2. XRD analysis

Bruker Eco D8 advanced Diffractometer was used to examine the character of AgNPs synthesized from *D. metel* Figure 2 showed the powder XRD diffraction pattern recorded in the 2θ range of 20-90°. This XRD pattern displays the number of Bragg reflections at 31.8°, 38.8°, 44.23°, 45.8°, 64.56°, 77.5° and 81.5°. Peaks exist at 38.8°, 44.23°, 64.56°, 77.5°and 81.5° characterizing the formation of AgNPs with polycrystalline nature, which are matches with standard JCPDS card No: 89-3722 with face-centered cubic crystal (fcc) system. Its fcc crystal model is shown in Figure 2. The characteristic peaks exhibited corresponding to crystalline orientations of (111), (200), (220), (311) and (222) hkl planes. The sharp and prominent peak at 38.8° illustrates the preferential growth orientation of AgNPs toward the (111) lattice planes. The similar kind of unassigned peaks at 2θ value of 27.75°, 31.8°, 40.6°, 45.8°, 54.4°, 57.4°, 67.5°, 74.3° and 85.2° were marked by # (Figure 2) symbol which indicates the organometallic complex phase of XRD pattern and may be coming from the leaf extract of *D. metel*. during on crystallization (Bhardwaj et al. 2016). In agreement with the Scherer formula, the average crystallite size of AgNPs was 40 nm.

3.3. FTIR analysis

The functional group of synthesized Ag NPs was analyzed through FTIR spectrometer Shimadzu IRTRACER-1100 at a wavelength range from 400-4000 cm^{-1} and their FTIR spectrum shows in Figure 3. with the characteristic peaks

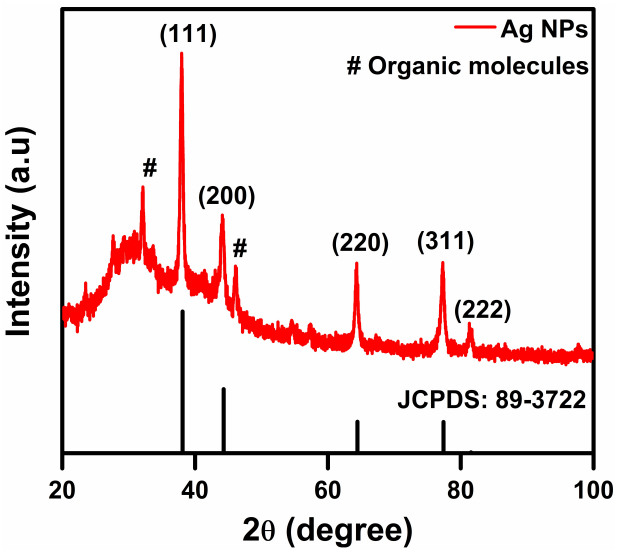

FIGURE 2 Powder XRD pattern of AgNPs synthesized from Datura metel L.

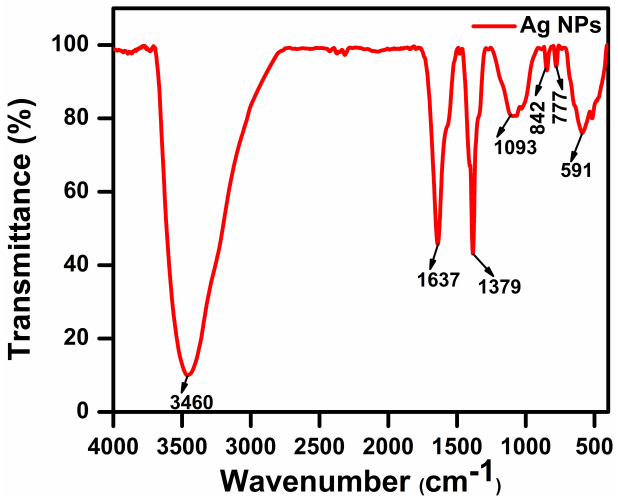

FIGURE 3 FTIR analysis of AgNPs.

at 3460, 1637, 1379, 1093, 842, 777 and 591 cm^{-1}. The absorption band at 3,460 cm^{-1} (OH stretching) showed the carboxylic group, while the peak at 1,637 cm^{-1} (C=C stretching) could be attributed to alkanes. The intense peak was found at 1,379 cm^{-1} (N=O bending) due to the amides, and a strong peak appeared at 1,093 cm^{-1} (–C-O stretching) associated with the phenolic acids. Two strong peaks emerged at 831 and 775 cm^{-1}, indicating the establishment of AgNPs. Generally, fingerprint regions of 400 cm^{-1} to 800 cm^{-1} belong to metal nanoparticles which support the existence peaks at 831 cm^{-1} and 775 cm^{-1} belonging to the synthesized AgNPs along with biomolecules. The broad absorption band at 591 cm^{-1} (C-H bending) reveals the existence alkyne (Bhardwaj et al. 2016). The functional groups C-H, C-C in D. metel leaf extract (identified in our previous study Chinnaiah et al. (2021)) do not observe, and the existence of a strong peak amide peak (1,379 cm^{-1}) and metal peak (775 cm^{-1}) in this spectrum confirms the formation of AgNPs. The amide and alkyl functional groups may be mainly responsible for reducing Ag precursor material.

3.4. SEM with EDAX analysis

Morphology of synthesized AgNPs was carried out by SEM (Model ZEISS-EVO 18, Japan) equipped with EDAX analysis. The SEM images of Ag nanoparticles at different magnifications are shown in Figure 4a, b and their EDAX analysis is shown in Figure 5, respectively. The image revealed that AgNPs have a clastic rock-like morphology, which has a small amount of agglomeration at some parts. The particle size found in the range of 508-857 nm was calculated from the SEM image using Image J software. The EDAX analysis confirmed the presence of Ag, that have a chemical composition of Na, Mg, S and Cl elements, which may come from leaf extract of *D. metel* and also found C, O is subject to the reference carbon at EDAX specimen, and atmosphere, respectively.

3.5. Cyclic voltammetry analysis

The supercapacitor performance of fabricated Ag electrode was analyzed at various scan rates (5-100 mV) using the three-electrode system in the potential limit of 0.3 to 0.65 V shown in Figure 6a. The CV graphs of the Ag electrode have anodic peaks that exist on positive current regions belonging to the oxidative process. Cathodic peaks have emerged on negative current regions corresponding to reduction reactions, revealing that the as-prepared electrodes are approved for the redox (oxidation-reduction) mechanism. However, the characteristic oxidation peaks occurred around 0.4 mV of the anodic cycle, and reduction peaks encircling on 0.11 mV of the cathodic cycle display the existence of Ag. The oxidation and reduction of individual Ag peak values (Ag-0.4mV) examine the redox characteristics of the Ag electrode. The CV graphs and their positions are increased during the variation of scan rate due to the diffusions of OH ions at the electrode/electrolyte interface. The CV graphs of Ag showed a predominant reduction peak may attribute to the oxidized state of Ag^{2+}. When making AgNPs, developing of the nearby fairly equal magnitude of oxidation, reduction peaks were expressed the complete oxidation of Ag into AgO by transformation two-electron reaction and could understand the compensation of oxidized behavior of Ag by the electron transfer process during the redox reaction. Moreover, all the obtained CV curves appeared as the regular shape displaying pseudo-capacitive behavior of as-prepared electrodes and have not changed their shape even on high scan rates indicating the as-prepared electrode has good rate capability, excellent reversibility and symmetric nature (Zhou et al. 2021). The shape of CV curves showed the redox mechanism of Ag electrode governed by the reversible faradic reaction. The possible redox mechanism of the fabricated Ag electrode during the redox reaction between the electrode and electrolyte could be expressed as follows.

$$Ag + OH^- \leftrightarrow AgOH + e^- \quad (4)$$

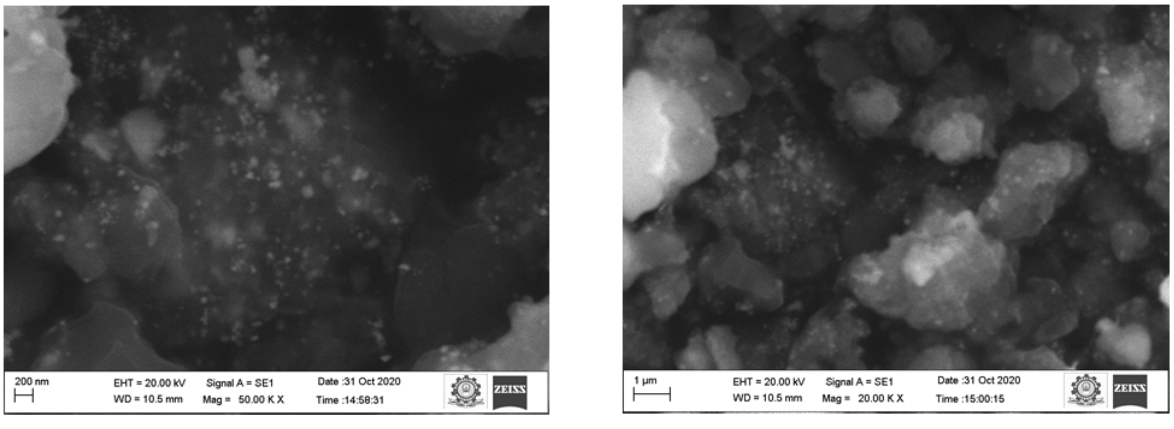

(a) (b)

FIGURE 4 SEM images. (a) Nanometer and (b) Micrometer Magnifications of AgNPs.

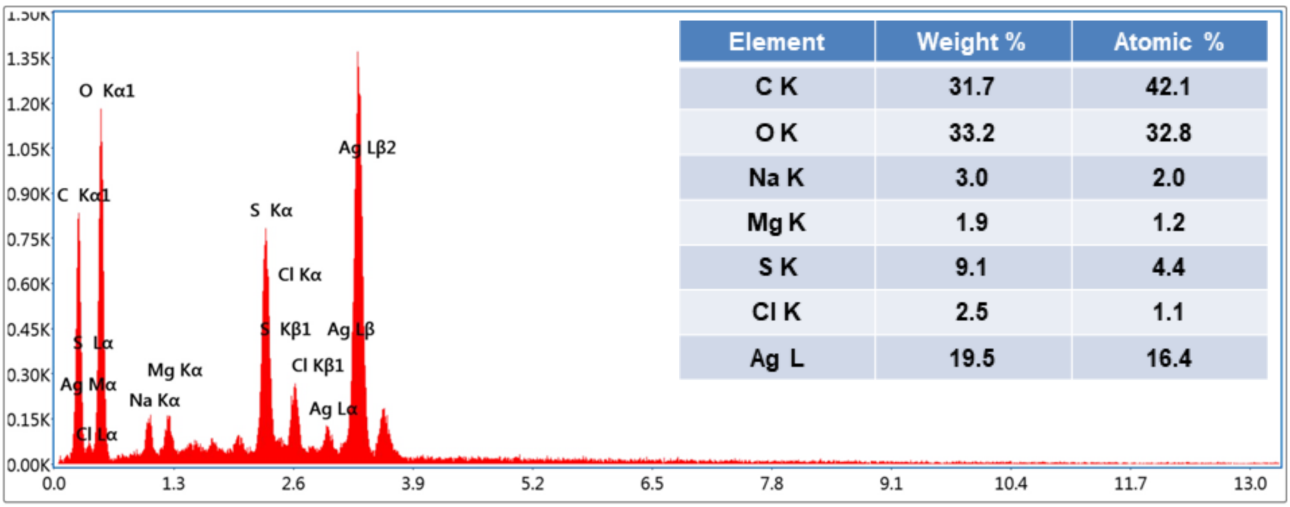

Element	Weight %	Atomic %
C K	31.7	42.1
O K	33.2	32.8
Na K	3.0	2.0
Mg K	1.9	1.2
S K	9.1	4.4
Cl K	2.5	1.1
Ag L	19.5	16.4

FIGURE 5 EDAX analysis of Ag nanoparticles.

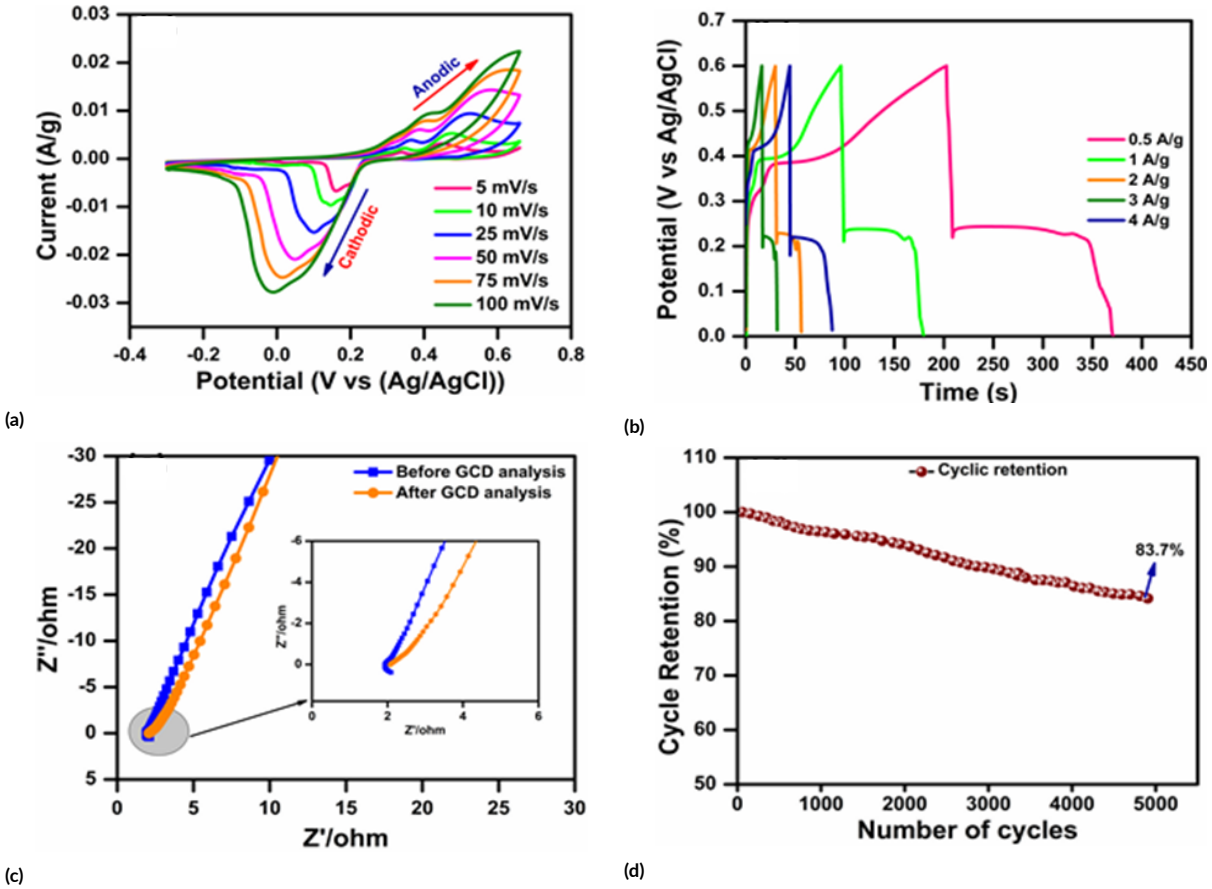

FIGURE 6 Electrochemical analysis a) cyclic voltammetry curves b) charge-discharge curves c) Nyquist plot d) cyclic retention of as prepared Ag electrode.

The faradic reversible reaction mechanism showed the involvement of Ag^+ ions activated by carbon molecules added during the slurry making on electrode preparation. When rising the scan rate, the magnitude of the first oxidation peak is shifted from 0.0015 A/g to 0.096 A/g at a scan rate of 5 to 100 mV, simultaneously their reduction peaks have gained some noticeable magnitude shifted from -0.006 A/g to -0.027 A/g for a corresponding scan rate of 5 to 100 mV/s respectively, which displays that linear relationship of magnitude and area of the CV curves (Ghadimi et al. 2019). The magnitude of the second oxidation (0.01 A) and reduction peak (0.29 A) was higher than that of pre-existing oxidation (0.009 A), reduction peak (0.27 A) might be caused by the reduction of Ag-

NPs. In addition, the successive redox cycles are bigger than the previous cycle advocating a certain amount of cations per cycle only from Ag involved in the action of the redox mechanism. Although redox peaks were shifted during the increment of scan rates from 5 - 100 mV, i.e., the oxidation peak moved from 0.338 to 0.415 mV concerning the higher positive potential side and their equal reduction peak moving from 0.155 to -0.019 mV respecting the lower negative potential side due to the sluggish electron transfer. Besides, it shows the exemplary contributions of the electrode-electrolyte kinetic process.

The superior specific capacitance of 251 F/g was achieved at a scan rate of 5 mV/s, which is more than the previous report. Kim et al. (2018) reported 115 F/g at a current density of 1 A/g for Ag/toner/paper electrode. All the remaining calculated specific capacitance values are 196, 150, 119, and 100 F/g for scan rates of 10, 25, 50, 75, and 100 mV/s. These suggested that diffusion of OH ions in electrolyte easily penetrates on inner portion and surface of the electrode and can create a more electrochemically active surface area at lower scan; hence more redox reaction occurred between the as-prepared Ag electrode and electrolyte. The organic trace elements, such as O, S, and C, in D. metel was identified in EDAX analysis and it might be one the reason for remarkably improved specific capacitance and which was an aid to keep up the stability of the electrode (Gao et al. 2019). However, greater scan rates exhibit the comparable low specific capacitance because of its less electroactive surfaces, which is caused by insufficient time of transportation of ions connecting the electrode and electrolyte and not easy access to the electrolyte ions on their surface, inner portions.

3.6. Choronopotentiometry analysis

The galvanostatic charge-discharge (GCD) characteristics of as-prepared Ag electrodes were studied in the potential limit of 0-0.6V at various current densities of 0.5–4 A/g. The obtained curves manifested in Figure 6b represent the non-reversible nature and indicate the pseudo-capacitive behavior of the Ag electrode by the electrochemical quasi-reversible redox reaction. All the obtained curves possess the IR drop, which may restrict the diffusion of OH ions at the surface of the electrode and similar kind of GCD behavior reported by previous literature (Zhou et al. 2021). The higher potential drop (incremental drop) found in all curves shows a decrement of charge diffusion at higher scan rates, which makes the quick redox reaction between electrode and electrolyte. Hence, the lowest current density of 0.5 A/g exhibits the longest discharge time due to switching more active surfaces by the OH^- ions diffusion. The higher specific capacitance of 267 F/g at a current density of 0.5 A/g displayed that more redox reaction takes place on low current density by the creation of a massed operative surface on the electrode, with remaining calculated specific capacitance of 186, 142, 126, and 115 F/g for a current density of 1, 2, 3 and 4 A/g consequently. At all the different current densities, the potential window of as-prepared electrodes Ag linearly increases during the charging process and linearly decreases during the discharge process revealing their good electrochemical properties. The slow current densities provide high specific capacitance by attributing more redox reactions of electrode surfaces and electrolytes. As prepared AgNPs have a clastic rock-like, morphology, these special features provide a more electroactive surface area by the transportation ions (Gao et al. 2021). The contribution of Ag/Ag^+ redox couple shows plateaus voltage found at 4 V in the GCD curve. Meanwhile, low scan rates and current densities foster the specific capacitance owing to the more diffusion of OH^- ions making a fresh active surface on an electrode. On another side, difficult to access the same OH^- ions at a higher scan rate and current density because of insufficient time of diffusion process to deliver less redox reaction (Asaithambi et al. 2021). The stability of the electrode was further checked by a long-term cyclic performance of AgNPs carried out by repeating the charge-discharge experiments for 5000 cycles and it shows the specific capacitance retention of 83.7%, indicating the excellent stability of the Ag electrode shown in Figure 6d.

3.7. EIS analysis

To realize the conducting behavior of as-prepared electrode Ag was carried out on EIS analysis measured from 1 Hz to 100 kHz. The Nyquist plot is expressed in Figure 6c, it was accounted for during the 5000 GCD cycles. The EIS spectra of the sample are involved in semicircle and straight lines on high-frequency and low-frequency regions respectively. The semicircles are found around on high-frequency domain, and their diameter of the loop is shown in Figure 6c exhibits the electrode kinetics of charge transfer (Rct) and intrinsic resistance (Rs) developed between the interfaces of electrode/electrolyte (Adhikari et al. 2020). In the high-frequency domain, the semicircle cut off in the x-axis shows the internal resistance between the electrode and electrolyte. The estimated internal resistances value of Ag is 2.3 Ω, which makes the same trend followed by their calculated values of charge transfer resistances typically 2.14 Ω after GCD analysis. The straight arrow hinge in the low-frequency domain is ascribed to the behavior of Warburg impedance; it could control the ions diffusions in the redox mechanism. The charge transfer resistance and solution resistance are working out from the EIS spectra fitting data through the Z-View software. The enlargement of curve fitting at the high-frequency region is shown in Figure 6c. The Ag electrode has smaller Rct values and is examined by the formation of consistent semicircles even before and after the cycle; it indicates more ions diffusion processes occurred between electrode and electrolyte. Meanwhile, it may relate to the clastic rock morphology of silver nanoparticles.

4. Conclusions

In summary, AgNPs were synthesized from leaf extract of *D. metel* as a reducing agent using the green synthesis

method. The XRD pattern showed the face-centered cubic crystal structure of prepared AgNPs with organometallic complex phase, while the FTIR spectra showed the presence of organic molecules and AgNPs. The clastic rock morphology observed from the SEM image and EDAX analysis affirms the presence of trace elements with Ag. The results obtained in this study show that synthesized AgNPs bind with trace elements and may utilize for deficiency-related biological applications. The specific capacitance of 267 F/g at 0.5 A/g and cyclic retention of 83.7% even after 5000 charge-discharge cycles demonstrate supercapacitor performance and clastic rock morphology synthesized AgNPs support the redox mechanism. Therefore, plant trace elements incorporated in AgNPs have a bright future in graphene hybrid supercapacitor as the electrochemical electrode.

Acknowledgments

The project was supported by Ministry of Science and Higher Education of Russia (Grant no. FENU-2020-0019). Authors (KC, KG) acknowledged Kalasalingam Academy of Research and Education, Krishnankoil, TamilNadu, India.

Authors' contributions

KK, VM, MK and KG designed the study. KC, SCJ, AM and DG carried out the laboratory work. KC, KK, VM, VP, MS and KG analyzed the data. KC, KK, VM and KG wrote the manuscript. All authors read and accepted the final version of the manuscript.

Competing interests

No conflict of interest.

References

Adavallan K, Gurushankar K, Nazeer SS, Gohulkumar M, Jayasree RS, Krishnakumar N. 2017. Optical redox ratio using endogenous fluorescence to assess the metabolic changes associated with treatment response of bioconjugated gold nanoparticles in streptozotocin-induced diabetic rats. Laser Phys. Lett. 14(6):065901. doi:10.1088/1612-202X/aa6b21.

Adhikari S, Selvaraj S, Ji SH, Kim DH. 2020. Encapsulation of Co*3O4* Nanocone Arrays via Ultrathin NiO for Superior Performance Asymmetric Supercapacitors. Small 16(48):1–13. doi:10.1002/smll.202005414.

Asaithambi S, Sakthivel P, Karuppaiah M, Balamurugan K, Yuvakkumar R, Thambidurai M, Ravi G. 2021. Synthesis and characterization of various transition metals doped SnO*2*@MoS*2* composites for supercapacitor and photocatalytic applications. J. Alloys Compd. 853:157060. doi:10.1016/j.jallcom.2020.157060.

Bhardwaj K, Kumar S, Ojha S. 2016. Antioxidant activity and FT-IR analysis of *Datura innoxia* and *Datura metel* leaf and seed methanolic extracts. African J. Tradit. Complement. Altern. Med. 13(5):7–16. doi:10.21010/ajtcam.v13i5.2.

Chinnaiah K, Maik V, Kannan K, Potemkin V, Grishina M, Gohulkumar M, Tiwari R, Gurushankar K. 2022. Experimental and Theoretical Studies of Green Synthesized Cu*2*O Nanoparticles Using *Datura metel* L. J. Fluoresc. 32(2):559. doi:10.1007/s10895-021-02880-4.

Chinnaiah K, Thivashanthi T, Asadi A, Muthuvel A, Kannan K, Gohulkumar M, Maik VK, Gurushankar. 2021. Recent advantages and applications of various biosynthesized greener silver nanoparticles. Asian J. Chem. 33(12):2871–2884. doi:10.14233/ajchem.2021.23392.

Gao X, Wang W, Bi J, Chen Y, Hao X, Sun X, Zhang J. 2019. Morphology-controllable preparation of NiFe*2*O*4* as high performance electrode material for supercapacitor. Electrochim. Acta 296:181–189. doi:10.1016/j.electacta.2018.11.054.

Gao X, Zhang H, Guo E, Yao F, Wang Z, Yue H. 2021. Hybrid two-dimensional nickel oxide-reduced graphene oxide nanosheets for supercapacitor electrodes. Microchem. J. 164:105979. doi:10.1016/j.microc.2021.105979.

Ghadimi LS, Arsalani N, Ahadzadeh I, Hajalilou A, Abouzari-Lotf E. 2019. Effect of synthesis route on the electrochemical performance of CoMnFeO*4* nanoparticles as a novel supercapacitor electrode material. Appl. Surf. Sci. 494:440–451. doi:10.1016/j.apsusc.2019.07.183.

Gurushankar K, Rimac H, Potemkin V, Grishina M. 2021. Investigation of the newly characterized baimantuoluoamide a and baimantuoluoamide b alkaloids as potential cyclin-dependent kinase 4 (CDK4) inhibitors using molecular docking and molecular dynamics simulations. J. Mol. Struct. 1230:129925. doi:10.1016/j.molstruc.2021.129925.

Gurushankar K, Shalini M, Mariappan G, Maik V, Chinnaiah K. 2020. Spectroscopic analysis of *Mollugo pentaphylla*, *Coldenia procumbenns*, *Cassia acutifolia*, *Achranthes aspere*. Int. J. Pharm. Res. 12:2314–2320. doi:10.31838/ijpr/2020.SP1.326.

Karuppiah D, Palanisamy R, Rengapillai S, Ponnaiah A, Marimuthu S. 2021. Effect of Tungsten and Carbon in Germanium Oxide as a High-Performance Electrode for Energy Storage Applications. ACS Appl. Energy Mater. 4(9):9692–9700. doi:10.1021/acsaem.1c01674.

Khan MA, Ahmad I, Ur Rahman I. 2007. Effect of environmental pollution on heavy metals content of *Withania somnifera*. J. Chinese Chem. Soc. 54(2):339–343. doi:10.1002/jccs.200700049.

Kim S, Yun TG, Kang C, Son MJ, Kang JG, Kim IH, Lee HJ, An CH, Hwang B. 2018. Facile fabrication of paper-based silver nanostructure electrodes for flexi-

ble printed energy storage system. Mater. Des. 151:1–7. doi:10.1016/j.matdes.2018.04.047.

Mistry H, Thakor R, Patil C, Trivedi J, Bariya H. 2021. Biogenically proficient synthesis and characterization of silver nanoparticles employing marine procured fungi *Aspergillus brunneoviolaceus* along with their antibacterial and antioxidative potency. Biotechnol. Lett. 43(1):307–316. doi:10.1007/s10529-020-03008-7.

Muthuvel A, Said NM, Jothibas M, Gurushankar K, Mohana V. 2021. Microwave-assisted green synthesis of nanoscaled titanium oxide: photocatalyst, antibacterial and antioxidant properties. J. Mater. Sci. Mater. Electron. 32(18):23522–23539. doi:10.1007/s10854-021-06840-3.

Stephane KD, Panta P, Shulga YM, Kumar A, Gupta M, Kumar Y. 2020. Physico-chemical characterization of activated carbon synthesized from *Datura metel*'s peels and comparative capacitive performance analysis in acidic electrolytes and ionic liquids. Bioresour. Technol. Reports 11:100516. doi:10.1016/j.biteb.2020.100516.

Tan JY, Liu Y, Cheng YG, Sun YP, Liu Y, Huang J, Guo S, Liu GZ, Kuang HX, Yang BY. 2020. Daturmetesides A-E, five new ergostane-type C28 sterols from the leaves of *Datura metel* L. Steroids 156:108583. doi:10.1016/j.steroids.2020.108583.

Zhou LX, Yang YY, Zhu HL, Zheng YQ. 2021. *In situ* synthesis of Ag/NiO derived from hetero-metallic MOF for supercapacitor application. Chem. Pap. 75(5):1795–1807. doi:10.1007/s11696-020-01431-8.